Acta Crystallographica Section A
Foundations and Advances
ISSN 2053-2733

Received 6 November 2013
Accepted 20 February 2014

Unified approach for determining tetragonal tungsten bronze crystal structures

M. Smirnov[a]* and P. Saint-Grégoire[b]

[a]Faculty of Physics, St Petersburg State University, Petrodvoretz, 194508 St Petersburg, Russia, and [b]Laboratoire MIPA, University of Nîmes, 30021 Nîmes cedex, France. Correspondence e-mail: smirnomb@rambler.ru

Tetragonal tungsten bronze (TTB) oxides are one of the most important classes of ferroelectrics. Many of these framework structures undergo ferroelastic transformations related to octahedron tilting deformations. Such tilting deformations are closely related to the rigid unit modes (RUMs). This paper discusses the whole set of RUMs in an ideal TTB lattice and possible crystal structures which can emerge owing to the condensation of some of them. Analysis of available experimental data for the TTB-like niobates lends credence to the obtained theoretical predictions.

1. Introduction

The theory of second-order structural phase transitions (SPTs) is based on the idea of the order parameter. In the case of displacive SPTs, the order parameter is a vector defining cooperative atomic displacements which describe the lattice deformation during the transformation from one phase to another. This deformation coincides (or almost coincides) with the eigenvector of the soft mode and possesses minimal mechanical stiffness. Hence, in order to determine the atomistic pattern of the order parameter for a particular SPT one should reveal the softest degree of freedom of the crystal lattice.

The crystal structures built on oxide frameworks are lattices formed by quasi-rigid XO_n polyhedra (tetrahedra, octahedra *etc.*), interconnected by common vertices or edges. It is possible that in such a structure there exist collective atomic displacements related to polyhedron translations and rotations and not involving any polyhedron deformations. Such deformations, called floppy modes (Cai & Thorpe, 1989) or rigid unit modes (RUMs; Hammonds *et al.*, 1996), are not accompanied by length variations of the $X-$O bonds and the O–O contacts. Thus, they are mechanically soft and potentially could play the role of soft-mode eigenvectors. It is notable that RUMs have no restoring forces only for infinitesimal deformations, *i.e.* within harmonic approximation (Gambhir *et al.*, 1997).

At larger atomic displacements they inevitably couple with the elastic strains. That is why the RUM-induced instabilities are often triggered by external pressure or by uniaxial compression (Mitra, 2004). A classic example of an SPT induced by an RUM soft mode is the ferroelastic SPT in the perovskite AXO_3 structure (Giddy *et al.*, 1993). The cubic perovskite (CP) structure is a framework of corner-sharing regular octahedra. In this structure, all RUMs involve concerted rotations of the octahedra located within a layer perpendicular to the rotational axis which may be parallel to the *a*, *b* or *c* axes. The first example of RUM-induced instability was the ferroelastic phase transition in $SrTiO_3$ (Shirane & Yamada, 1969). Much attention was paid to the RUM-induced 'compressibility collapse' in the cation-free CP oxide crystal ReO_3 (Mirgorodsky & Smirnov, 1993) and fluoride ScF_3 (Morelock *et al.*, 2013). The family of perovskite-like ferroelastics has now enlarged considerably. It includes various complex oxides (titanates, zirconates, aluminates, tantalates *etc.*) which display a wide variety of physical properties such as superconductivity, magnetism, ferroelectricity and magnetoelectricity, which make them very interesting for applications (Schranz, 2011).

Tetragonal tungsten bronze (TTB) oxides constitute one of the most important classes of ferroelectrics next to perovskites. They can also be viewed as framework lattices consisting of corner-sharing NbO_6 octahedra. However, the manner of the octahedra arrangement within a layer of the TTB structure (see Fig. 1*a*) differs from that in a perovskite structure, first by its lower symmetry (Jamieson *et al.*, 1968). In the *c* direction, the layers within a TTB lattice are repeatedly interconnected by sharing the apex octahedral corners. It is seen that within this layer-like framework lattice there are pentagonal, square and trigonal tunnels which can accommodate cations of different sizes, respectively, denoted as $M^{(5)}$, $M^{(4)}$ and $M^{(3)}$. Thus the net formula can be written as $M_i^{(5)}M_j^{(4)}M_k^{(3)}Nb_{10}O_{30}$. Because of the large choice of the inserted cations, the TTB family presents a rich sequence of phase transitions and includes a large number of functional crystals and materials possessing electro-optic, pyroelectric and piezoelectric properties (Uchino, 2000).

Many TTB structures undergo ferroelastic SPTs which transform the tetragonal lattice into orthorhombic ones. The tetragonal-to-orthorhombic distortions are usually weak and in some cases manifest themselves *via* incommensurate (INC) structure modulations. It seems reasonable to suggest that the

ferroelastic transformations in TTB crystals may also be related to an RUM tilting deformation. In this crystalline family, the important role of octahedral tilting was emphasized (Levin *et al.*, 2006). However, a detailed analysis of the whole RUM spectrum in the TTB structure and the variety of possible crystal structures induced by their condensation has not yet been done.

This paper aims to fill this gap. It is organized as follows. First, we describe a novel theoretical approach to the enumeration of RUMs in an arbitrary framework crystal. The approach is illustrated and justified by application to the previously well studied CP structure. Subsequently, the approach is used to determine the complete set of RUMs in the TTB lattice. Then, all crystal structures that could arise from an ideal tetragonal TTB lattice as a result of condensation of various RUMs are specified. Finally, these results are compared with experimentally determined crystal structures of the niobate TTB-like crystals.

Because of the large variability in filling the cation positions, the 'tungsten bronzes' comprise a great family of compounds, even larger than the perovskites. Thus, the approach developed in the paper will be useful to rationalize, to interpret and even to predict the structural constitution of a large family of crystals of scientific and applied interest. An additional point to emphasize is that the novel approach to enumeration of RUMs may be used equally well for other crystallographic systems.

2. Method

The whole set of RUM-induced structures originating from cubic perovskite was described by Glazer (1972). As an elementary RUM deformation he considered the concerted octahedron tilting around one of the lattice axes. The octahedral rigidity condition strictly connects the tilting of octahedra localized within the same layer perpendicular to the axis of rotation but does not constrain rotations of octahedra localized within different such layers. Thus the octahedra of neighbouring layers may tilt in-phase, anti-phase or even with arbitrary phase shift. Glazer introduced notations $a+$, $a-$, $b+$, $b-$, $c+$ and $c-$ for the in-phase and anti-phase octahedron rotations, respectively, around axes oriented along the a, b and c axes. It is noteworthy that the tilting deformations around mutually perpendicular axes are independent. Thus, any possible RUMs in a perovskite lattice can be determined by a triad $\varphi_a, \varphi_b, \varphi_c$ with components determining the phase shifts between tilt angles of neighbouring layers perpendicular to the a, b and c axes.

Depending on the combination of $\varphi_a, \varphi_b, \varphi_c$ values, various crystal structures can be obtained from the cubic perovskite structure. A detailed analysis of such structures for the case $\varphi_i = 0, \pi$ was presented in Glazer (1972). Many of them were later observed for particular perovskite-like compounds. In some cases, the octahedral tilting deformations really play the role of the order parameter for ferroelastic phase transitions.

Later on, the concept of concerted tilting of rigid polyhedra was generalized to be applicable for arbitrary framework

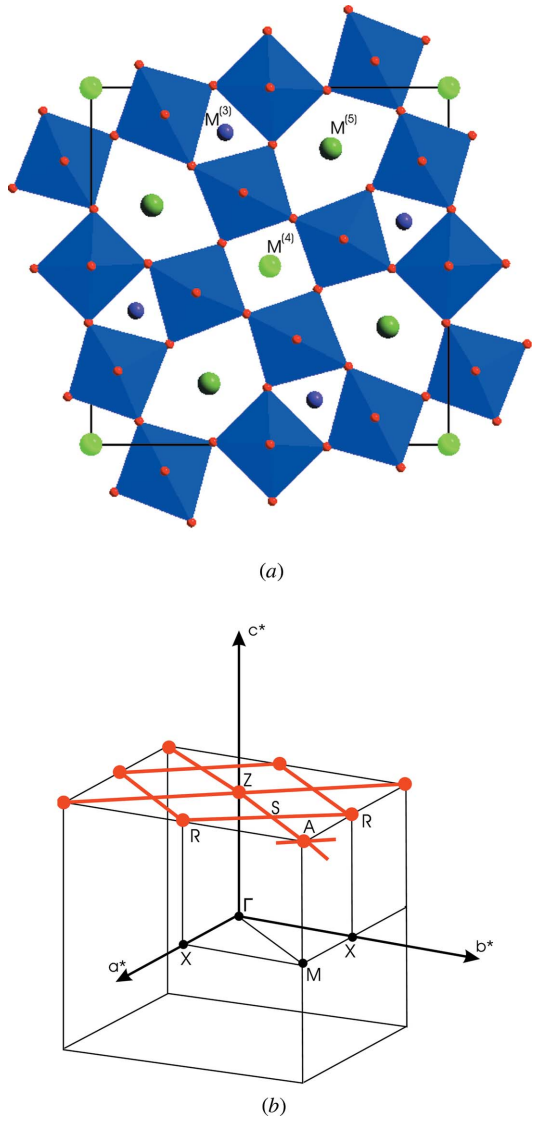

Figure 1
Structure (*a*) and Brillouin zone (BZ) (*b*) of an ideal TTB crystal.

structures (Swainson & Dove, 1993). In that paper, the notion of the RUM as a phonon mode which does not involve any structural distortions except polyhedron rotations and translations was clearly formulated.

The question has arisen – how to determine the whole set of RUMs for an arbitrary crystal structure? The split-atom model was proposed to solve this problem (Giddy *et al.*, 1993). The essence of this approach is to view each polyhedron as a separate rigid body and to treat the linked corners as kept together by harmonic springs. We consider this method somewhat unnecessarily complicated, especially for polyatomic structures.

We propose an alternative approach, which consists of direct simulation of the phonon modes of a framework lattice built of rigid XO_n polyhedra. Such a method resembles the computational scheme used previously for simulation of floppy modes in the network glasses (Cai & Thorpe, 1989). That method was based on the harmonic potential function in terms of valence bonds and valence angles. Assuming finite

stiffness of these coordinates, the model retains zero stiffness of the floppy modes. This approach can be used in studying RUMs in the framework lattices. However, in this case it can be simplified by assuming finite stiffness of larger structural units – the entire XO_n polyhedra.

In order to ensure rigidity of the polyhedra, it is sufficient to postulate stiffness of the polyhedron's O–O edges. For doing this, one can assume that the apex O atoms are linked by Hooke's springs. All other atoms but O should be omitted. Hooke's stiffness coefficient K is the only free parameter of the model. Its value must be taken so that $\lambda_0 = K/M$ (here M is the mass of O atoms) will be much higher than the numerical accuracy of the diagonalization procedure used.

Construction of the dynamical matrix for such a model lattice can be readily done as follows. Let indexes k and l numerate atoms in the unit cell, and indexes α and β denote Cartesian components. If atoms k and l are linked by a polyhedron edge $\mathbf{R}$ then the corresponding component of the force constant matrix is determined by the expression

$$D_{k\alpha,l\beta}(\mathbf{q}) = \lambda_0 \exp\left[i\mathbf{q}\cdot(\mathbf{r}_k - \mathbf{r}_l)\right] G_{k\alpha,l\beta}, \qquad (1)$$

in which $\mathbf{r}_k$ and $\mathbf{r}_l$ are atomic positions in the same unit cell and G is a dimensionless structure-dependent tensor:

$$G_{k\alpha,l\beta}(\mathbf{q}) = \sum_{\mathbf{R}_{kl}} \frac{R_{kl,\alpha}R_{kl,\beta}}{R_{kl}^2} \exp(i\mathbf{q}\cdot\mathbf{R}_{kl}). \qquad (2)$$

Summation in equation (2) is over all polyhedron edges connecting atoms k and l. For $\mathbf{q} = 0$ and $k = l$ the G-matrix elements (self-interaction terms) are defined as follows:

$$G_{k\alpha,k\beta}(0) = -\sum_{l\neq k} G_{k\alpha,l\beta}(0). \qquad (3)$$

Upon diagonalization of the $\mathbf{D}(\mathbf{q})$ matrix one obtains $3N$ eigenvalues $\lambda_n(\mathbf{q})$ which correspond to squared phonon frequencies. The essence of the proposed approach consists of scanning $\mathbf{q}$ vectors over the whole Brillouin zone (BZ) and selecting the modes with zero frequencies. All these modes are RUMs. Their eigenvectors and corresponding $\mathbf{q}$ values do not depend on particularities of the chosen potential model but only on structural particularities of the lattice under study. A simple but instructive example provides us with an application of this method to the cubic perovskite lattice (see Appendix).

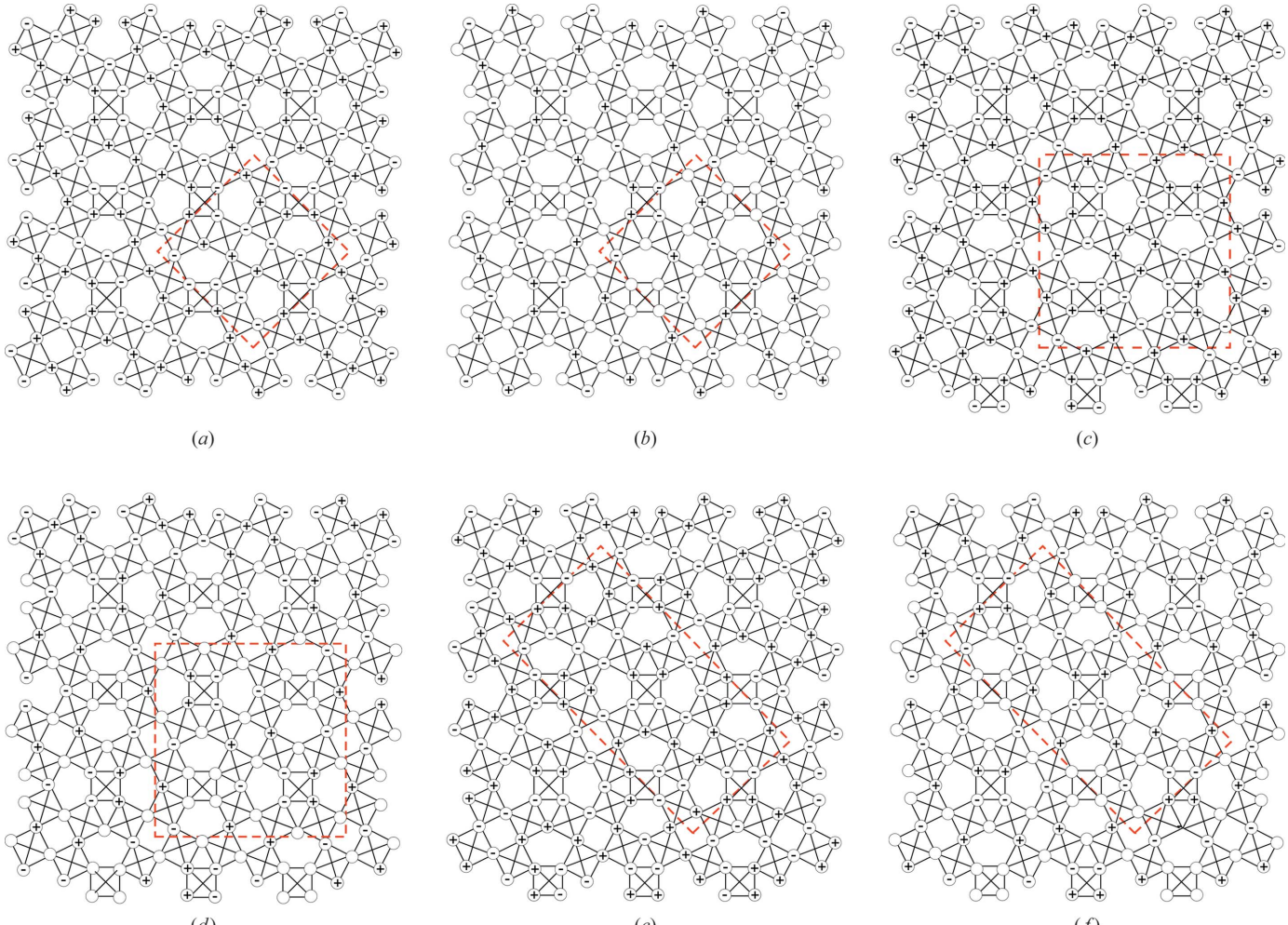

Figure 2
Eigenvectors of RUMs. Z RUMs: ρ^+/ρ^+ (*a*) and $\rho^+/0$ (*b*). A RUMS: ρ^-/ρ^- (*c*) and $\rho^-/0$ (*d*). R RUMs: σ^+/σ^+ (*e*) and $\sigma^+/0$ (*f*). Dashed lines show unit cells of resulting substructures. The cations are not shown for simplicity.

3. Results and discussion

3.1. Atomistic pattern of RUMs in TTB

The starting aristotype structure is tetragonal with *P*4/*mbm* symmetry. Most of the TTB-like compounds crystallize in this structure at high temperature. The unit cell of this lattice and the corresponding BZ are shown in Figs. 1(*a*) and 1(*b*). A detailed presentation of the TTB structure can be found elsewhere, see for example Jamieson *et al.* (1968). Special points within the BZ are $Z = \left(00\frac{1}{2}\right)$, $A = \left(\frac{1}{2}\frac{1}{2}\frac{1}{2}\right)$, $R = \left(0\frac{1}{2}\frac{1}{2}\right)$. For all these points, the calculations revealed the existence of two RUMs. Moreover, the calculations indicated the presence of two RUM branches along the *Z*–*A* and *R*–*S*–*R* directions. Eigenvectors of the RUMs belonging to the special BZ points are shown in Fig. 2. Spatial patterns of these modes seem rather complicated. Nevertheless, they can be classified in a simple way as follows. A detailed analysis of the *Z* and *A* RUMs shown in Figs. 2(*a*)–2(*d*) leads to the conclusion that they can be represented as combinations of ρ deformations shown in Fig. 3(*a*). Analogously, the *R* RUMs shown in Figs. 2(*e*)–2(*f*) can be represented as combinations of σ deformations shown in Fig. 3(*b*).

It is remarkable that both ρ and σ deformations shown in Fig. 3 are localized in the layers perpendicular to (110) or the (1$\bar{1}$0) direction. Thus, arbitrary combination of such ρ and σ deformations localized in different layers would give rise to an RUM. The situation is analogous to that in the CP lattice. The only difference is that, in a CP lattice, because of the higher symmetry, the RUM-containing layers are stacked in three directions (100), (010) and (001), whereas in the TTB lattice they can be stacked only in two directions. It is important to note that the ρ and σ deformations localized in mutually perpendicular layers do not overlap (in the sense that they involve displacements of different atoms). Hence, any combination of ρ and σ deformations localized in the (110) layers may be accompanied by arbitrary combination of similar deformations localized in the (1$\bar{1}$0) layers, thus giving rise to manifold different RUMs.

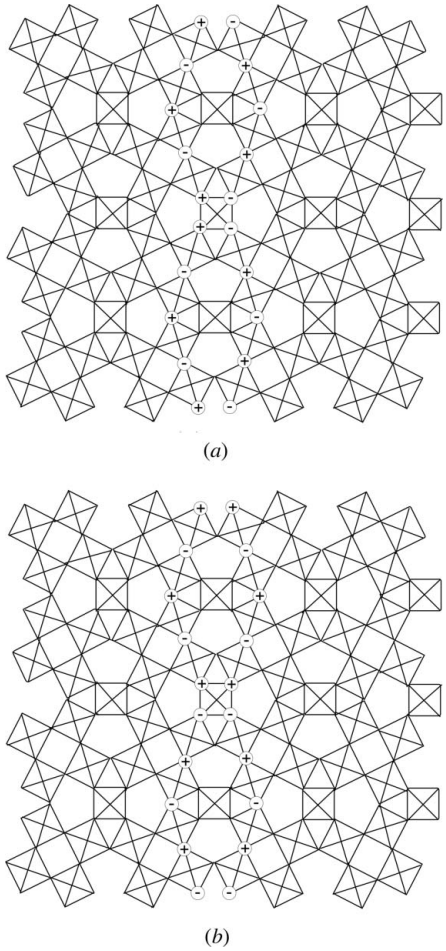

Figure 3
Two types of RUMs localized in the (110) layer: ρ RUM (*a*) and σ RUM (*b*).

Analyzing the CP lattice, Glazer considered the RUMs resulting from the in-phase and anti-phase combinations of octahedron rotations localized in neighbouring layers. They were labelled by indexes '+' and '−' attached to the vector determining the layer orientation. Similarly, one can use the notation σ^+, ρ^+, σ^- and ρ^- when describing the RUM deformations in a TTB lattice. These symbols determine the type and consequence of the concerted octahedron rotations. In order to specify completely the RUM distortion in a TTB lattice, one must define these symbols for the two perpendicular directions (110) and (1$\bar{1}$0). Below we use pairs of the symbols separated by a slash. Zero denotes the absence of deformations. Thus, the modes shown in Figs. 2(*a*) and 2(*b*) must be denoted as ρ^+/ρ^+ and $\rho^+/0$, respectively; the modes in Figs. 2(*c*) and 2(*d*) are denoted as ρ^-/ρ^- and $\rho^-/0$, respectively; the modes in Figs. 2(*e*) and 2(*f*) as σ^+/σ^+ and $\sigma^+/0$, respectively.

It should be recognized that all the above-discussed *Z*, *A* and *R* RUMs are doubly degenerated. For example, the two mutually orthogonal *Z* RUMs are $\rho^+/0$ and $0/\rho^+$ (or ρ^+/ρ^+ and $\rho^+/-\rho^+$). Thus, any combination of these modes will also be a *Z* RUM. This fact opens up the possibility of the existence of combined $x\rho^+/y\rho^+$ RUMs (here $x \neq y$). Similarly $x\rho^-/y\rho^-$ and $x\sigma^+/y\sigma^+$ would give rise to *A* RUMs and *R* RUMs, respectively.

The above notations allow us to describe the RUM phonon branches along *Z*–*S*–*A* and *R*–*S*–*R* directions. Thus, the *Z*–*S*–*A* branch in *Z* and *A* points includes the $\rho^+/0$ and $\rho^-/0$ modes, respectively. In the intermediate *k*-points, the phonons of this branch correspond to the $\rho(\varphi)/0$ modes, where φ is the phase shift varying between 0 and π. Similarly, the RUM branch along the *R*–*S*–*R* direction consists of the $\sigma(\varphi)/0$ modes, which vary continuously between $\sigma^+/0$ and $\sigma^-/0$. The presence of the whole RUM branches may result in the occurrence of the INC structures with modulation vectors $(\xi, \xi, 0)$ and $\left(\xi, \bar{\xi}, 0\right)$. Thus, the whole set of RUMs in the TTB lattice includes the *Z*–*S*–*A* and *R*–*S*–*R* phonon branches each including one RUM. These lines are highlighted in Fig. 1(*b*) in red. The special points *Z*, *A* and *R* are cross-points of two such lines. Thus, there are two doubly degenerated RUMs belonging to these points. Point *S* is also the cross-point of two RUM branches of a different atomistic pattern. This fact can be considered as a kind of accidental degeneracy.

Table 1
Substructures resulting from the single RUM condensation.

a, **b**, **c** are unit-cell vectors of the parent tetragonal structure and $\mathbf{a}_s$, $\mathbf{b}_s$, $\mathbf{c}_s$ are unit-cell vectors of the resulting substructures. IR = irreducible representation.

k-point and IR	RUM	$\mathbf{a}_s$, $\mathbf{b}_s$, $\mathbf{c}_s$	Substructure
$Z = (00\frac{1}{2})$ IR $Z5^+$	ρ^+/ρ^+	**a**, **b**, 2**c**	*Pbnm* (No. 62)
	$\rho^+/0$	**a** − **b**, **a** + **b**, 2**c**	*Ccmm* (No. 63)
	$x\rho^+/y\rho^+$	**a**, **b**, 2**c**	$P112_1/m$ (No. 11)
$A = (\frac{1}{2}\frac{1}{2}\frac{1}{2})$ IR $A5^+$	ρ^-/ρ^-	**a** − **b**, **a** + **b**, 2**c**	*I*4/*m* (No. 87)
	$\rho^-/0$	**a** − **b**, **a** + **b**, 2**c**	*Ibmm* (No. 74)
	$x\rho^-/y\rho^-$	**a** − **b**, **a** + **b**, 2**c**	*C*112/*m* (No. 12)
$R = (0\frac{1}{2}\frac{1}{2})$ IR *R*1	σ^+/σ^+	**a**, 2**b**, 2**c**	$A2_1am$ (No. 36)
	$\sigma^+/0$	**a**, 2**b**, 2**c**	*A*112/*m* (No. 12)
	$x\sigma^+/y\sigma^+$	**a**, 2**b**, 2**c**	*A*11*m* (No. 8)

Table 2
Substructures resulting from condensation of two RUMs.

k-points	RUM	$\mathbf{a}_s$, $\mathbf{b}_s$, $\mathbf{c}_s$	Substructure
Z, *A*	ρ^+/ρ^-	**a** − **b**, **a** + **b**, 2**c**	*Pcmn* (No. 62)
Z, *R*	ρ^+/σ^+	**a**, 2**b**, 2**c**	$P112_1/m$ (No. 11)
A, *R*	ρ^-/σ^+	2**a**, 2**b**, 2**c**	*P*112/*m* (No. 10)
S, *R*	$\rho^+\rho^-/\sigma^+$	2(**a** − **b**), **a** + **b**, 2**c**	*Bbmm* (No. 63)
S, *S*	$\rho^+\rho^-/\sigma^+\sigma^-$	2(**a** − **b**), 2(**a** + **b**), 2**c**	*B*112/*m* (No. 12)

3.2. Substructures induced by RUM condensation

In this section we analyze crystal structures resulting from the condensation of different RUMs (we call them *substructures*). RUMs related to different combinations of the ρ and σ rotations are listed in Table 1. Special *k*-points and irreducible representations of the RUM phonons are listed in the first column of Table 1. Particular combinations of the ρ and σ RUMs are shown in the second column and the resulting substructures are characterized in the third and fourth columns.

The structures resulting from condensation of these RUMs are specified by defining their unit-cell vectors and the space-symmetry groups. In this paper we focus our attention on the RUMs in the special *k*-points. All of them give rise to the substructures with twofold unit cells. Condensation of RUMs with longer modulation lengths (corresponding to other *k*-points) will result in the occurrence of more complex substructures.

In view of the forthcoming discussion of the experimental data, it is interesting to consider substructures which result from simultaneous condensations of two RUM modes. Some of them are listed in Table 2.

The structures listed in Tables 1–2 can be considered as resulting from the ideal tetragonal TTB lattice due to the condensation of one or two RUMs, *i.e.* in the course of a ferroelastic SPT. To our knowledge, no compound with the TTB structure undergoes a ferroelastic SPT directly from the tetragonal *P*4/*mbm* para-phase structure. For all such compounds, the ferroelastic SPT is preceded by a ferroelectric SPT. The sequence of SPTs observed on lowering temperature is usually as follows: para-phase → ferroelectric → ferroelectric/ferroelastic.

The low-temperature structures reported in the literature correspond to ferroelectric ferroelastic phases. The hypothetical substructures listed in Tables 1–2 correspond to structures resulting from the para-phase *via* a ferroelastic SPT. In order to compare them with the structures determined experimentally, we must take into account structural distortions induced by ferroelectric SPTs. In fact, there is a good reason to think that structural distortions induced by ferroelastic and ferroelectric transformations are not coupled. Indeed, the former consists of concerted octahedron rotations (*i.e.* primarily involves displacements of oxygen atoms), and the latter involves primarily displacements of the cation atoms from their symmetric positions in the centres of the lattice voids as well as niobium-atom displacements from the centres of octahedra. The symmetry reduction induced by a possible ferroelectric distortion polarized along a given direction can be easily taken into account by eliminating the symmetry operations which do not keep this direction invariant. Subgroups determined thus are listed in Table 3.

Table 3
Space groups of ferroelastic ferroelectric substructures for different polarization directions.

		Spontaneous polarization direction		
a_s, b_s, c_s	Ferroelastic substructures	$\mathbf{a}_s$	$\mathbf{b}_s$	$\mathbf{c}_s$
1, 1, 2	D_{2h}^{16} *Pbnm* (62)	C_{2v}^{2} *P*21*am* (26)	C_{2v}^{2} *Pb*21*m* (26)	C_{2v}^{9} *Pbn*21 (33)
$\sqrt{2}$, $\sqrt{2}$, 2	D_{2h}^{17} *Ccmm* (63)	C_{2v}^{14} *C*2*mm* (38)	C_{2v}^{14} *Cm*2*m* (38)	C_{2v}^{12} *Ccm*21 (36)
$\sqrt{2}$, $\sqrt{2}$, 2	C_{4h}^{5} *I*4/*m* (87)	C_{2}^{3} *I*112 (5)	C_{2}^{3} *I*112 (5)	C_{4}^{5} *I*4 (79)
$\sqrt{2}$, $\sqrt{2}$, 2	D_{2h}^{28} *Ibmm* (74)	C_{2v}^{20} *I*2*mm* (44)	C_{2v}^{22} *Ic*2*m* (46)	C_{2v}^{22} *Ibm*2 (46)
1, 2, 2	C_{2v}^{12} $A2_1am$ (36)	C_{2v}^{12} $A2_1am$ (36)	C_{s}^{3} *A*11*m* (8)	C_{s}^{4} *A*1*a*1 (9)
1, 2, 2	C_{2h}^{3} *A*112/*m* (12)	C_{s}^{3} *A*11*m* (8)	C_{s}^{3} *A*11*m* (8)	C_{2}^{3} *A*112 (5)
$\sqrt{2}$, $\sqrt{2}$, 2	D_{2h}^{16} *Pcmn* (62)	C_{2v}^{2} *P*21*ma* (26)	C_{2v}^{9} *Pc*21*n* (33)	C_{2v}^{2} *Pcm*21 (26)
1, 2, 2	C_{2h}^{2} $P112_1/m$ (11)	C_{s}^{1} *P*11*m* (6)	C_{s}^{1} *P*11*m* (6)	C_{2}^{2} $P112_1$ (4)
2, 2, 2	C_{2h}^{1} *P*112/*m* (10)	C_{s}^{1} *P*11*m* (6)	C_{s}^{1} *P*11*m* (6)	C_{2}^{1} *P*112 (3)
$2\sqrt{2}$, $\sqrt{2}$, 2	D_{2h}^{17} *Bbmm* (63)	C_{2v}^{12} *Bm*2*m* (35)	C_{2v}^{12} *Bb*21*m* (36)	C_{2v}^{16} *Bbm*2 (40)
$2\sqrt{2}$, $2\sqrt{2}$, 2	C_{2h}^{3} *B*112/*m* (12)	C_{s}^{3} *B*11*m* (8)	C_{s}^{3} *B*11*m* (8)	C_{2}^{3} *B*112 (5)

3.3. Overview of crystal structures of TTB-like niobates

Some of the structures listed in Table 3 can be found among crystal structures discovered experimentally for various TTB niobate compounds. Some of these compounds are listed in Table 4. Crystal structures of these compounds are collected in Table 5.

Comparing Tables 5 and 3, one can draw the following conclusions:

(i) The RUM-induced structures should be accompanied by a doubling of the unit cell in the *c* direction. Hence, the structures 1–4 and 7 (No. in Table 5) cannot be directly related to any RUM-induced ferroelastic structure.

Table 4
List of the TTB-like crystalline niobates.

Re = Bi, La, Nd, Sm and Gd.

Compound	Notation
$Ba_4Na_2Nb_{10}O_{30}$	BNN
$(Ba_{0.67}Sr_{0.33})_5Nb_{10}O_{30}$	BSN
$(Sr_{0.67}Ba_{0.33})_5Nb_{10}O_{30}$	SBN
$Pb_4K_2Nb_{10}O_{30}$	PKN
$Pb_2K_4Li_2Nb_{10}O_{30}$	PKLN
$(Ca_{0.28}Ba_{0.72})_5Nb_{10}O_{30}$	CBN
$(Ba_{0.67}Re_{0.33})_5(TiNb)_{10}O_{30}$	BRTN

(ii) With the exception of structures shown in the first line of Table 3, unit-cell parameters of the RUM-induced structures should differ from those of the parent tetragonal structure. Hence, the structures 1–3 and 11 cannot be directly related to any RUM-induced ferroelastic structure.

(iii) Structures 5, 8 and 9 can be truly considered as RUM-induced structures.

(iv) The structure *Bmm*2 is very close to the RUM-induced structure *Bbm*2. In fact, the latter was considered in Bursill & Lin (1987) as a possible alternative but was rejected (in our opinion erroneously).

(v) The structure *Im*2*a* is equivalent to the RUM-induced structure *Ic*2*m* but corresponds to twice larger *a* and *b* parameters. This may be caused by a hidden commensurate structure modulation.

The RUM distortions are soft. They are numerous among the phonon states of a TTB-like lattice. Therefore, they can give rise to various structural fluctuations, static as well as dynamic. Such fluctuations may condense in a regular periodic superstructure or may induce an INC modulation. Equally, the structural fluctuations may lead to a state with a random spatial distribution having a static or a dynamic character. In such a case, they would result in unusually large and highly anisotropic atomic displacement parameters or even may appear in the results of crystal structure resolution as a spatial split of some atomic positions.

Table 5
Crystal structures of TTB niobates according to experimental data.

No.	Compound	Space group	a_s, b_s, c_s	SP direction	Order/ disorder	Reference
1	BNN, BSN, PKLN	*P*4*bm* (100)	1, 1, 1	$\mathbf{c}_s$	Order	I, II, III
2	BNN, PKLN	*Pba*2 (32)	1, 1, 1	$\mathbf{c}_s$	Order	I, IV
3	SBN	*P*4*bm* (100)	1, 1, 1	$\mathbf{c}_s$	Disorder	V, VI
4	BNN	*Cmm*2 (35)	$\sqrt{2}$, $\sqrt{2}$, 1	$\mathbf{c}_s$	Disorder	VII
5	BNN, SBN	*Ccm*21 (36)	$\sqrt{2}$, $\sqrt{2}$, 2	$\mathbf{c}_s$	Order	VIII, IX
6	SBN, CBN	*Bmm*2 (38)	$\sqrt{2}$, $2\sqrt{2}$, 2	$\mathbf{c}_s$	Order INC	IX, X
7	PKN	*Cm*2*m* (38)	$\sqrt{2}$, $\sqrt{2}$, 1	$\mathbf{b}_s$	Order	XI
8	BNN	*Bbm*2 (40)	$2\sqrt{2}$, $\sqrt{2}$, 2	$\mathbf{c}_s$	Order	XII
9	SBN	*Im*2*a* (46)	$2\sqrt{2}$, $2\sqrt{2}$, 2	$\mathbf{b}_s$	Order	XIII
10	BRTN	*Im*2*a* (46)	$\sqrt{2}$, $\sqrt{2}$, 2	$\mathbf{c}_s$	Order	XIV
11	SBN	*P*4*bm* (100)	1, 1, 2	$\mathbf{c}_s$	INC	XV

I, Foulon *et al.* (1996); II, Podlozhenov *et al.* (2006); III, Elaatmani *et al.* (2003); IV, Gagou *et al.* (2001); V, Jamieson *et al.* (1968); VI, Chernaya *et al.* (1997); VII, Jamieson *et al.* (1969); VIII, Toledano (1975); IX, Bursill & Lin (1987); X, Lu *et al.* (2006); XI, Sciau *et al.* (1999); XII, Labbe *et al.* (1989); XIII, Bursill & Lin (1987); XIV, Levin *et al.* (2006); XV, Woike *et al.* (2003).

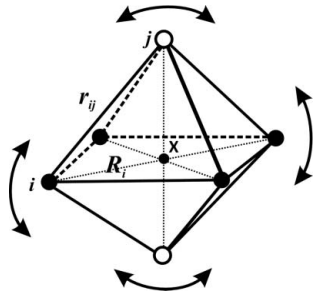

Figure 4
The octahedron as a basic structural unit of the TTB structure. The apex and equatorial oxygen atoms are shown by open and filled circles, respectively. Atomic oscillations involved in RUMs are shown by arrows.

Atomic displacements during the tilting oscillations of octahedra involved in RUMs are shown in Fig. 4 by arrows. It is clear that the equatorial oxygen atoms (shown as filled circles) have maximal amplitudes in the vertical direction (along the *c* axis) and the apex oxygen atoms (shown as open circles) have maximal amplitudes in the horizontal direction (in the *ab* plane). One can find similar relations between atomic displacement parameters in the published TTB structures which do not involve the *c* parameter doubling (Podlozhenov *et al.*, 2006; Elaatmani *et al.*, 2003). In all cases when the anisotropic mean square amplitudes were determined, the amplitudes of equatorial oxygen atoms were found markedly larger in the *c* direction and those of the apex oxygen atoms are larger in the perpendicular direction. This fact allows us to suggest the presence of a hidden structural disorder, static or dynamic. The latter case implies large-amplitude oscillations dictated by RUMs.

Structures with split oxygen positions merit a special discussion. The presence of such splittings suggests that the reported structure is in fact an average of two (or several) ordered structures corresponding to opposite signs of RUM distortions. A detailed analysis of such disordered structures leads to the determination of possible ordered constituents. The disordered *Cmm*2 structure (the case of $Ba_2NaNb_5O_{15}$, BNN) proposed in Jamieson *et al.* (1969) is an example. According to the chosen combination of RUM signs it can be represented as an average of two ordered *Ccm*21 structures or of two ordered *Bbm*2 structures.

In some studies, structures of the TTB crystals were determined as belonging to the *P*4*bm* space group. This is a ferroelectric structure with a polar axis parallel to (001). Such a structure may be thought to originate from the para-electric phase without any ferroelastic distortion. However, diffraction experimental data and subsequent structure refinements (Podlozhenov *et al.*, 2006; Elaatmani *et al.*, 2003; Jamieson *et al.*, 1968) show that in these structures the oxygen thermal amplitudes are considerably anisotropic, which is quite consistent with a mechanism of condensation of RUMs as discussed above. Moreover, the

presence of an INC modulation was found in some SBN structures (Levin *et al.*, 2006; Woike *et al.*, 2003; Schefer *et al.*, 2008) and it is remarkable that the directions of this modulation were found to be (110) and (1$\bar{1}$0). This is in full agreement with our suggestion of possible RUM-induced INC structure variations.

4. Summary and conclusion

Lattice dynamics calculations reveal the existence of rigid unit modes in TTB crystal lattices. These phonon modes can be represented as spatially modulated combinations of the elementary vibrations. These are concerted rotations of the octahedra localized in narrow layers perpendicular to the (110) and (1$\bar{1}$0) directions. This particularity results in the occurrence of two RUM phonon branches along the *R*–*S*–*R* and *X*–*S*–*L* lines in the BZ of a TTB lattice.

The RUM-induced substructures, *i.e.* crystal structures resulting from an ideal tetragonal TTB lattice owing to the condensation of different RUMs, are specified. The analysis of available experimental data for TTB-like niobate crystals showed that some of these structures do coincide with the RUM-induced structures. Other cases, with disordered atomic positions, may be interpreted as being due to the condensation of several RUMs and would thus correspond to structures averaged over several RUM-induced structures. This novel result allows us to suggest that the proposed scheme of RUM-induced structures will be useful for the unified classification of TTB-related crystal structures.

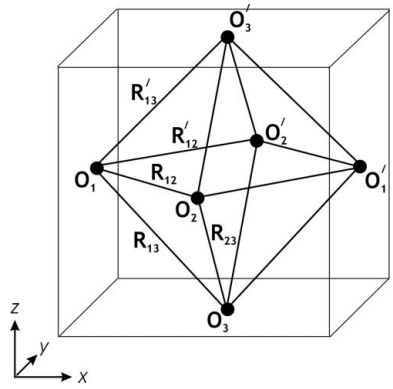

Figure 5
Unit cell of the cubic perovskite XO_3 framework lattice.

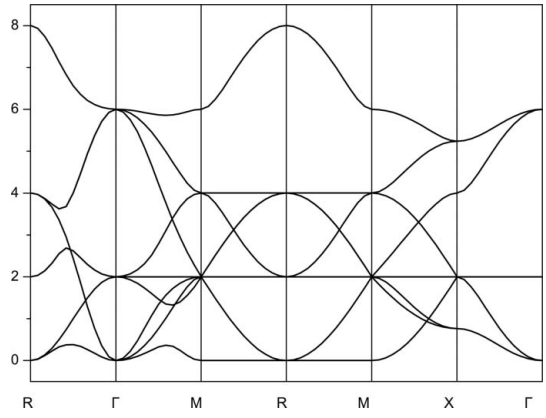

Figure 6
The $\lambda_n(\mathbf{q})$ dependencies calculated for the cubic perovskite XO_3 framework lattice at $\lambda_0 = 1$.

APPENDIX *A*

As an example, let us consider the cubic perovskite lattice. There are three O atoms per unit cell. Every O atom belongs to two octahedra and forms eight O–O edges (see Fig. 5). For example, every O1 atom forms four O1–O2 and four O1–O3 edges *etc.* Thus, the sums in equation (1) include four terms. Accomplishing the summation, one obtains the *G* matrix which can be represented in block form:

$$\mathbf{G} = \begin{pmatrix} \mathbf{G}_{11} & \mathbf{G}_{12} & \mathbf{G}_{13} \\ \mathbf{G}_{12} & \mathbf{G}_{22} & \mathbf{G}_{23} \\ \mathbf{G}_{13} & \mathbf{G}_{23} & \mathbf{G}_{33} \end{pmatrix},$$

where

$$\mathbf{G}_{12} = \begin{pmatrix} A_{xy} & B_{xy} & 0 \\ B_{xy} & A_{xy} & 0 \\ 0 & 0 & 0 \end{pmatrix}, \quad \mathbf{G}_{13} = \begin{pmatrix} A_{xz} & 0 & B_{xz} \\ 0 & 0 & 0 \\ B_{xz} & 0 & A_{xz} \end{pmatrix},$$

$$\mathbf{G}_{23} = \begin{pmatrix} 0 & 0 & 0 \\ 0 & A_{yz} & B_{yz} \\ 0 & B_{yz} & A_{yz} \end{pmatrix},$$

$$A_{\alpha\beta} = -\cos\left(\tfrac{1}{2}q_\alpha a\right)\cos\left(\tfrac{1}{2}q_\beta a\right),$$

$$B_{\alpha\beta} = \sin\left(\tfrac{1}{2}q_\alpha a\right)\sin\left(\tfrac{1}{2}q_\beta a\right)$$

and *a* is the unit-cell parameter.

We fixed $\lambda_0 = 1$ and diagonalized the *D* matrix for the $\mathbf{q}$ vector running over different symmetry directions within the BZ. The calculated $\lambda_n(\mathbf{q})$ dependencies are shown in Fig. 6. It is seen that the condition $\lambda_n(\mathbf{q}) = 0$ is fulfilled at *M* and *R* points [$\mathbf{q} = (\frac{1}{2}, \frac{1}{2}, 0)$ and $\mathbf{q} = (\frac{1}{2}, \frac{1}{2}, \frac{1}{2})$] and along the whole *M*–*R*–*M* lines. This result agrees with the conclusions obtained previously within the split-atom approach (Giddy *et al.*, 1993).

The authors would like to thank V. Kazimirov and T. Smirnova for preparation of the figures. We thank also the Conseil Régional Languedoc Roussillon (France) for financing an invited professor position for one of us (M. Smirnov). This study was partly supported by the Russian Foundation for Basic Research (project No. 12-03-01140-a).

References

Bursill, L. A. & Lin, P. J. (1987). *Acta Cryst.* B**43**, 49–56.
Cai, Y. & Thorpe, M. F. (1989). *Phys. Rev. B*, **40**, 10535–10542.
Chernaya, T. S., Maksimov, B. A., Verin, I. V., Ivleva, L. I. & Simonov, V. I. (1997). *Crystallogr. Rep.* **42**, 375–380.
Elaatmani, M., Zegzouti, A., Capitelli, F., Moliterni, A. G. G., Migliori, A. & Calestani, G. (2003). *Z. Kristallogr.* **218**, 26–31.

Foulon, G., Ferriol, M., Brenier, A., Boulon, G. & Lecocq, S. (1996). *Eur. J. Solid State Inorg. Chem.* **33**, 673–686.
Gagou, Y., Mezzane, D., Aliouane, N., Fabry, J., Badeche, T., Zegzouti, A., Lopez, M. & Saint-Gregoire, P. (2001). *Ferroelectrics*, **251**, 131–137.
Gambhir, M., Heine, V. & Dove, M. T. (1997). *Phase Transit.* **61**, 125–139.
Giddy, A. P., Dove, M. T., Pawley, G. S. & Heine, V. (1993). *Acta Cryst.* A**49**, 697–703.
Glazer, A. M. (1972). *Acta Cryst.* B**28**, 3384–3392.
Hammonds, K. D., Dove, M. T., Giddy, A. P., Heine, V. & Winkle, B. (1996). *Am. Mineral.* **81**, 1057–1079.
Jamieson, P. B., Abrahams, S. C. & Bernstein, J. L. (1968). *J. Chem. Phys.* **48**, 5048–5057.
Jamieson, P. B., Abrahams, S. C. & Bernstein, J. L. (1969). *J. Chem. Phys.* **50**, 4352–4363.
Labbe, P., Leligny, H., Raveau, B., Schneck, J. & Toledano, J. C. (1989). *J. Phys. Condens. Matter*, **2**, 25–43.
Levin, I., Stennett, M. C., Miles, G. C., Woodward, D. I., West, A. R. & Reaney, I. M. (2006). *Appl. Phys. Lett.* **89**, 122908.
Lu, C. J., Qi, Y. J., Li, J. Q., Zhang, H. J. & Wang, J. Y. (2006). *Appl. Phys. Lett.* **89**, 191901.
Mirgorodsky, A. P. & Smirnov, M. B. (1993). *J. Phys. Condens. Matter*, **5**, 3313–3324.
Mitra, S. (2004). *High Pressure Geochemistry and Mineral Physics*, Vol. 9, *Basics for Planetology and Geo-Material Science (Developments in Geochemistry)*. Amsterdam: Elsevier.
Morelock, C. R., Greve, B. K., Gallington, L. C., Chapman, K. W. & Wilkinson, A. P. (2013). *J. Appl. Phys.* **114**, 213501.
Podlozhenov, S., Graetsch, H. A., Schneider, J., Ulex, M., Wöhlecke, M. & Betzler, K. (2006). *Acta Cryst.* B**62**, 960–965.
Schefer, J., Schaniel, D., Petricek, V., Woike, T., Cousson, A. & Woehlecke, M. (2008). *Z. Kristallogr.* **223**, 399–407.
Schranz, W. (2011). *Phys. Rev. B*, **83**, 094120.
Sciau, Ph., Calvarin, G. & Ravez, J. (1999). *Acta Cryst.* B**55**, 459–466.
Shirane, G. & Yamada, Y. (1969). *Phys. Rev.* **177**, 858–863.
Swainson, I. P. & Dove, M. T. (1993). *Phys. Rev. Lett.* **71**, 193–196.
Toledano, J. C. (1975). *Phys. Rev. B*, **12**, 943–950.
Uchino, K. (2000). *Ferroelectric Devices.* New York, USA: Marcel Dekker.
Woike, T., Petříček, V., Dušek, M., Hansen, N. K., Fertey, P., Lecomte, C., Arakcheeva, A., Chapuis, G., Imlau, M. & Pankrath, R. (2003). *Acta Cryst.* B**59**, 28–35.